

ITERA: IDL Tool for Emission-line Ratio Analysis

Brent A. Groves^a, Mark G. Allen^b

^a*Sterrewacht Leiden, Leiden University, Neils Bohrweg 2, Leiden 2333-CA The Netherlands*

^b*Observatoire de Strasbourg UMR 7550 Strasbourg 67000, France*

Abstract

We present a new software tool to enable astronomers to easily compare observations of emission line ratios with those determined by photoionization and shock models, ITERA, the IDL Tool for Emission-line Ratio Analysis. This tool can plot ratios of emission lines predicted by models and allows for comparison of observed line ratios against grids of these models selected from model libraries associated with the tool. We provide details of the libraries of standard photoionization and shock models available with ITERA, and, in addition, present three example emission line ratio diagrams covering a range of wavelengths to demonstrate the capabilities of ITERA. ITERA, and associated libraries, is available from <http://www.brentgroves.net/itera.html>.

Keywords: hydrodynamics - shock waves - ISM: abundances,- Galaxies: Nuclei, Galaxies: Seyfert - infrared: ISM, Ultraviolet: ISM, X-rays: ISM

1. Introduction

All emission lines are sensitive to some extent on the physical conditions in the emitting gas. This includes the density and electron temperature of the medium, the abundance of the emitting element, and the details of the ionizing source such as the luminosity and effective temperature of the star in H II regions. While both atomic and line theory and observational data have advanced sufficiently over the years such that the dependency of individual emission lines on nebulae parameters is known, determining these same parameters from individual lines is difficult apart from a few exceptions. One of the simplest ways to break these inherent degeneracies is through the use of emission line ratios. Using lines arising from the same elements, or similar ionization potentials, or even from different levels of the same ion, can minimize the dependence on some or most of the parameters that control line emission, thus enabling the construction of diagnostics.

One of the first diagnostic emission line ratios was the [O III] line ratio $\lambda 4363\text{\AA}/\lambda 5007\text{\AA}$ put forward by Menzel et al. (1941). By using forbidden

lines of the same ion, O⁺², both the abundance and ionization dependencies are removed, leaving a ratio strongly dependent on electron temperature due to the different excitation levels of the lines involved (see e.g. Fig. 2.5 in Dopita & Sutherland, 2003). This line method, and other methods of determining electron temperature, have been discussed in detail by Peimbert (1967). The same reasoning has also been extended to several other line ratios, using lines from a single ion but arising from different energy levels, such as optical-IR ratios like [O III] $\lambda 5007\text{\AA}/\lambda 52\mu\text{m}$ (see e.g. Dinerstein et al., 1985) and UV ratios like C III] $\lambda 1909/\text{C III}\lambda 977$.

Similarly, ratios of forbidden lines arising from the same ion and similar energy levels remove abundance, ionization and temperature dependencies. If these lines arise from levels with different collisional de-excitation rates or radiative transition probabilities, this ratio will be sensitive to the densities in the range spanned by the critical densities of the lines involved. This idea was first put forward by Aller et al. (1949) for the [O II] doublet, $\lambda 3726/\lambda 3729$, and has been extended to several other strong lines like [S II] $\lambda 6716/\lambda 6731$ or in the IR [S III] $\lambda 18.7\mu\text{m}/\lambda 33.5\mu\text{m}$ (see Rubin, 1989, for a nice overview of these ratios).

Apart from the temperature and density sen-

Email addresses: brent@strw.leidenuniv.nl (Brent A. Groves), allen@astro.u-strasbg.fr (Mark G. Allen)

sitive ratios described above, determining physical quantities from single line ratios proves difficult due to degeneracies between the various controlling parameters of the nebula emission. Generally what is done is to use several line ratios in combination to break these degeneracies, such as determining the metallicity or abundances in the gas (see e.g. Kewley & Ellison, 2008, for an overview of several line methods for metallicity determination), or to use empirically-based assumptions, such as the constancy of the Balmer decrement in H II regions for dust-reddening determination (also theoretically supported, see e.g. Cox & Mathews, 1969; Brocklehurst, 1971; Miller & Mathews, 1972, though these concentrate mostly on planetary nebulae). An overview of all methods of comparing observed emission lines with theory can be found in Stasińska (2007) and in books such as Osterbrock & Ferland (2006) and Dopita & Sutherland (2003), which give a broad understanding of the topic and underlying physics.

One of the best ways to disentangle these degeneracies is to plot two line ratios against each other in what is commonly called a line diagnostic diagram. These were first used as a method to distinguish various classes of emission-line galaxies in Heckman (1980) and Baldwin et al. (1981), with the diagrams described in the latter still commonly used to distinguish star-forming or H II galaxies from galaxies dominated by an active galactic nucleus (AGN). These diagrams for emission-line galaxy classification were revised and extended by Veilleux & Osterbrock (1987), who based their selection of line ratios on 5 criteria: Line strength (1), Line proximity (for blending (2) and reddening (3) effects), the preferable inclusion of hydrogen lines (4) and the capability of detecting these lines (5).

With improvements in the availability of spectra, with wavelengths from the UV (such as Hubble-STIS) to FIR (e.g. Herschel -PACS & -HIFI) available, increased spectral sensitivity and resolution, and a copious number of ionization models now available (e.g. Morisset, 2008), such criteria need not be so strict. However, these large increases in wavelength range, sensitivity, and models make analysis of emission-line objects much more complicated.

It is for these reasons that we introduce here a new, publicly available, emission-line analysis tool, ITERA. ITERA, the IDL Tool for Emission-line Ratio Analysis, allows the simple comparison of observed emission-lines from UV to far-IR wave-

lengths to models to assist in the determination of properties such as gas density, metallicity and excitation mechanism. We describe in the following sections the code and demonstrate some of the possible diagnostic diagrams available.

2. The ITERA Program

The IDL Tool for Emission-line Ratio Analysis (ITERA) had its inception with the SHOCKPLOT tool created to display the results of the Allen et al. (2008) 150–1000 km s⁻¹ shock models. The power of such a tool was quickly realised and the original tool was rewritten and expanded into its current form. ITERA is an IDL¹ widget tool which enables astronomers to plot line ratio diagrams of emission lines arising from atomic and ionized species as determined by standard photoionization and shock models. It also allows for a comparison of these line ratios with those obtained from observations or other models. As discussed in the introduction, these diagrams, or the individual ratios of the diagram, can be used as diagnostics of nebulae excitation mechanisms, nebulae density, electron temperature, metallicity or individual abundance variations, and other model-specific parameters. ITERA can also be used to determine line sensitivities to such parameters, thus giving the possibility of creating new or “best possible” diagnostics for a given set of observations. It can even be used to estimate line fluxes that are weak or in unobserved wavelength ranges.

ITERA works in three simple steps; the user selects the emission lines to be used as the denominators and numerators of the ratios for the X- and Y- axes, selects the model(s) that the user wants to examine, and, if wished, the user enters observational data for comparison. These steps can be performed in any order. Multiple lines can be chosen for the ratios in the case of emission line doublets or line blends due to resolution or velocity effects. What is returned is an emission-line ratio diagram of the chosen ratios, displaying a grid of the chosen models and, if entered, observational data points. This diagram can be printed, or the model

¹IDL, the Interactive Data Language, is a computing environment for data analysis, visualization, and application development, available from ITT Visual Information Solutions (<http://www.ittvis.com/ProductServices/IDL.aspx>).

grids displayed can be output for use in other routines, or direct comparison with data. The program and associated libraries and routines are available from <http://www.brentgroves.net/itera.html>. An IDL virtual machine² version is also available for those without access to IDL licences. Full instructions and details of the program are found on the webpage, but we describe below the major parts of the program.

The principle of ITERA is to allow ease of access for astronomers to existing shock- and photoionization models for the determination of emission line strengths. Thus the strength of ITERA lies in the library of shock- and photoionization models associated with the code. This library is a distinct yet necessary part of ITERA, needed to generate the line ratios. As the library is not an integral part of ITERA, only the desired model series need to be downloaded and installed (such as AGN or H II-region models, with further models added later as required, including photoionization models generated by the user.

2.1. Choosing the Models

The library of models associated with ITERA cover the range of excitation mechanisms expected within emission-line galaxies; star formation, active galactic nuclei and shocks. These models, generated by the shock and photoionization code MAPPINGS III, broadly cover the ratio space occupied by the dominant optical emission lines from galaxies. Other sources of emission lines, such as individual O and B stars (H II regions) or planetary nebulae, can be included through the user-generated option of ITERA, and may be included in the library at a later date. The ITERA model library is split into four main categories: Starburst or stellar ionization models, AGN models, shock models, and user-generated models. The currently available libraries are shown in table 1, and described briefly below.

ITERA has the possibility of plotting up to any number of shock or photoionization model grids, although for clarity the number displayed on any plot is generally limited to 5. Every model set has a limited number of parameters, with common parameters to the models being the emitting gas metallicity or abundance pattern, and the gas density

or pressure. The other parameters associated with the models tend to be specific to the specific sets, either due to the different physics associated with the ionizing/excitation mechanism, or due to different definitions by the model set creators. These include the hardness of the radiation field, the velocity of a shock ionizing the gas, or the dimensionless photoionization parameter. The parameters associated with the different model sets within the ITERA model library are described in the following subsections.

The model grids displayed within the ITERA plot window are formed by the ranges of two of these parameters, with the other parameters of the model sets fixed. The fixed parameters thus describe the different model grids that can be plotted. The first parameter of the model grid is set and cannot be chosen by the user, and is generally a measure of the ionization state of the gas, such as ionization parameter or shock velocity. The second parameter of the grid can be chosen by the user, with the choice of density, metallicity or the unique parameter associated with that model set (as described below). If the user of ITERA wants to compare parameters other than the set first parameter, e.g the ionization parameter, this can be done by simply limiting the parameter range to a single value and plotting multiple grids.

2.1.1. Starburst Models

The ITERA model library includes 3 different Starburst models, aimed specifically at galaxies whose line emission is dominated by gas ionized by recent ($< 10^7$ yr) star formation, generally classified as starburst, H II, or star-forming galaxies. However, these models can also be generally applied to any massive star formation region, though the comparison may break down for less massive star formation regions once the effects of the stochastic sampling of the stellar initial mass function becomes important ($\lesssim 10^4 M_{\odot}$).

The first model set is from Kewley et al. (2001). These models use stellar ionizing spectra generated by the stellar population synthesis codes PEGASE-2 (Fioc & Rocca-Volmerange, 1997) and Starburst99 (Leitherer et al., 1999), and considers both continuous star formation and instantaneous bursts. These models are then passed through the MAPPINGS III code for a range of ionization parameters³. The stellar models

²IDL virtual machine is free runtime version of IDL available from <http://www.itvis.com/ProductServices/IDL/VirtualMachine.aspx>

³The ionization parameter, q , also known as the ioniza-

Starburst models
Kewley et al. (2001) models
<ul style="list-style-type: none"> • Pegase2 stellar models <ul style="list-style-type: none"> ◦ Instantaneous Star Formation ◦ Continuous Star Formation • Starburst99 stellar models <ul style="list-style-type: none"> ◦ Instantaneous Star Formation ◦ Continuous Star Formation
Levesque et al. (2010) models
<ul style="list-style-type: none"> • Standard mass loss stellar models <ul style="list-style-type: none"> ◦ Instantaneous Star Formation ◦ Continuous Star Formation • High mass loss stellar models <ul style="list-style-type: none"> ◦ Instantaneous Star Formation ◦ Continuous Star Formation
Dopita et al. (2006) \mathcal{R} parameter models
AGN models
Standard, constant density, dust-free, photoionized AGN
Dusty, Radiation-Pressure dominated, photoionized AGN
Shock Models
Shock ionized cloud
Photoionized Precursor
Shock+Precursor
User-generated models
User run Cloudy & MAPPINGS III photoionization models

Table 1: Listing of the model libraries currently available with ITERA

and subsequent photoionization modelling are determined for 5 metallicities, ranging from 0.05 to 2.0 Solar (Z_{\odot}). For full details see the Kewley et al. (2001) paper. These models were used as a basis for the strong-line metallicity estimators in Kewley & Dopita (2002) and for the empirical/theoretical AGN/star-formation dividing lines discussed in Kauffmann et al. (2003) and Kewley et al. (2006).

The second set of models is from Levesque et al. (2010), and is an updated version of the Kewley et al. (2001) models, using a later version of MAPPINGS III (version IIIr) code for the radiative transfer, and using the latest version of the Starburst99 code (Vázquez & Leitherer, 2005). Like the Kewley et al. (2001) work, Levesque et al. (2010) model includes both instantaneous burst and continuous star formation stellar models, and covers a similar range in ionization parameter, q , and metallicity. In addition, the Levesque et al. (2010) models also cover a range of ages between 0 to 10 Myr (in steps of 0.5 Myr). What distinguishes these models from previous works is that they examined two different evolutionary tracks for the stellar populations, one with a standard mass loss treatment (STD) and one with high mass loss rates (HIGH) meant to more accurately match observations (see Levesque et al., 2010, for full details about the different tracks and the models).

The third set is the “ \mathcal{R} parameter” models of Dopita et al. (2006). As with the previous set, these use MAPPINGS IIIr for the radiative transfer and the latest version of Starburst99 to generate the ionizing stellar spectra, though only instantaneous bursts were considered. The same range of stellar ages and metallicities as Levesque et al. (2010) are used. What differentiates these models from the previous sets is that a direct link with the stellar populations and the surrounding ionized gas is considered. In these models all stellar clusters are born buried within their molecular birth clouds, but, over time, they clear an empty bubble around them, sweeping up the gas that forms the surrounding H II regions. This means that there is a direct link of both the gas density and incident ionizing flux, and thus the ionization parameter, at the inner edge of the H II region to the evolution of the

tion front speed, is a measure of the ionizing photon flux over the (hydrogen) gas density; $q = S_*/n_{\text{H}}$, where S_* is the integral of the photon flux above 13.6 eV. This is also often given in a dimensionless form; $U = q/c$.

stars. With this link, the time-averaged ionization parameter is found to be directly correlated with the mass of the ionizing cluster divided by the average ISM pressure, defined within the Dopita et al. (2006) work as \mathcal{R} ($= M_{\text{cl}}/P_{\text{ISM}}$). Thus it is this \mathcal{R} parameter rather than the local ionization parameter, q , that is measured when the emission-line ratios are measured on galactic scales. For full details about the \mathcal{R} parameter and the models see Dopita et al. (2006).

One important caveat with these models is that, while all three use the same global metallicities, the elemental abundances at each metallicity for each model differ due to the evolving definition of the abundance pattern at solar metallicity. Thus such differences must be considered when comparing these models. In table 2 we list the solar abundance patterns used in all models of the ITERA library discussed here. Most abundances are the same, except for oxygen which was recalibrated between different model sets (see e.g. Asplund et al., 2005). Different metallicities simply scale as multiples of the abundances listed here, except for helium and nitrogen, a secondary element (see Groves et al., 2004a). One cautionary note on the abundances listed here is that these do not take account of the effects of dust depletion, which varies amongst the models (from non-existent to significant), which will alter the gas-phase abundances.

Element	Kewley2000	Levesque2010	\mathcal{R} param	AGN models	Shocks
H.....	0.00	1.00	0.00	0.00	0.00
He.....	1.01	-1.01	-1.01	-0.99	-1.01
C.....	-3.44	-3.59	-3.59	-3.61	-3.44
N.....	-3.95	-4.22	-4.22	-4.20	-3.95
O.....	-3.07	-3.34	-3.34	-3.31	-3.07
Ne.....	-3.91	-3.91	-3.91	-3.92	-3.91
Na.....		-5.75		-5.68	
Mg.....	-4.42	-4.47	-4.47	-4.42	-4.42
Al.....		-5.61		-5.51	-5.53
Si.....	-4.45	-4.49	-4.49	-4.49	-4.45
S.....	-4.79	-4.79	-4.79	-4.80	-4.79
Cl.....		-6.40		-6.72	
Ar.....	-5.44	-5.20	-5.20	-5.60	-5.44
Ca.....	-5.64	-5.64	-5.64	-5.65	-5.88
Fe.....	-4.33	-4.55	-4.55	-4.54	-4.63
Ni.....		-5.68		-5.75	

Table 2: Solar abundances used in ITERA Libraries, given as $\log_{10}(X/H)$.

2.1.2. AGN Models

The library of AGN models used in the ITERA code are those from the Groves et al. (2004a,b) photoionization models of the narrow line regions of AGN. We include two series of AGN models, the classic dust-free, AGN power-law ionized models and the dusty, radiation pressure dominated models introduced by Groves et al.. Both of these models use simple power-law radiation fields ($f_\nu \propto \nu^\beta$) to represent the AGN ionizing spectrum, and explore the same range in metallicities (with the same abundance patterns), gas densities and ionization parameters. However the first models are dust free and assume a constant gas density throughout the narrow line region cloud. The second set are taken to be isobaric (constant pressure) and include dust and the effects of radiation pressure on dust, which causes significant differences in the resulting emission line spectrum at high ionization parameters (see Groves et al., 2004a,b, for full details of the models). These latter models are much more closely matched with the observed line ratio space and are the recommended model to use.

While these models do not represent the full range of theoretical models for the emission from the narrow line regions of AGN (see e.g., Binette et al., 1996; Ferguson et al., 1997), they do broadly cover the expected emission of strong emission lines, and can be used to estimate the “AGN space” of line ratios.

2.1.3. Shock Models

The shock models used in the ITERA library are directly imported from the Allen et al. (2008) work on fast shocks. They include a range of metallicities, densities, and magnetic parameters (the “unique parameter” of these models), and explore velocities from ~ 150 to 1000 km s^{-1} , where strong J-shocks occur. The shock models are split into three sets. The first is the emission from the post-shock region, where gas is shock-excited to high temperatures and ionization states. The second model set is from the pre-shock or precursor region which is photoionized by the radiation emitted upstream from the post-shock region. The third set is the combination of these (shock+precursor) for integrated measurements where the individual regions cannot be distinguished. For full details on the parameters and underlying physics of the models see Allen et al. (2008).

2.1.4. User Generated Models

While the above models cover the expected parameter space of emission-line galaxies, they are not representative of individual objects, where variations in the abundances of specific elements, ionizing source variations or even geometrical effects can all affect the final emission-line spectrum. Therefore we include the final option of user generated model libraries. This allows the possibility of a user inputting the results from well tested and respected photoionization codes such as Cloudy⁴ (Ferland et al., 1998) and MAPPINGS III⁵ (Groves et al., 2004a), or using on-line interfaces such as `mapiionline`: <http://www.ifa.hawaii.edu/~kewley/Mappings/>. For a listing, comparison, and benchmarking of such models see Péquignot et al. (2001), though all these models have advanced since this work.

To assist in the input of user generated models into ITERA, we provide tools for converting the outputs from these models to format used by ITERA. Currently only conversion tools for the publicly available codes Cloudy and MAPPINGS III are provided, but this may be expanded at a later date depending on demand.

2.2. Choosing Line Ratios

In principle, the choice of emission lines to use in the diagnostic line ratios in ITERA is limited purely by those provided by the code used to generate the photoionization/shock model. In MAPPINGS III (including all the models provided in the library) this is limited to ~ 1770 emission lines in the infrared, optical, and ultraviolet, and even including high-ionization/inner-shell lines in the X-ray. In Cloudy, this is further expanded by a host of weaker lines as well as molecular ro-vibrational emission lines from CO and H₂. The lines are listed in simple selection boxes, with only strong lines listed by default, though all lines, or lines in certain wavelength ranges, can be displayed if wished.

In addition, sums of lines can be used in the line ratios to account for line blending at low spectral resolution, or to account for different levels or ionization states (i.e. [O II] $\lambda 3726 + 3729$).

⁴Cloudy is available for download from <http://www.nublado.org>, along with full details on the code, how to use it, and how it works.

⁵MAPPINGS III is available to download from <http://www.brentgroves.net/mapiii.html>, which includes a description of the code and its use.

In practice however, the guidelines discussed in the introduction form the bases for good diagnostics. Lines of the same element and of the same ionization state or of similar excitation potential in different elements provide some of the strongest diagnostics. Lines relative to hydrogen recombination lines are also good diagnostics. As discussed in Veilleux & Osterbrock (1987), lines in close wavelength proximity limit the possible instrumental, calibration, and reddening effects.

Hence it is for this reason that several standard, strong-line, diagnostic ratios, such as $[\text{S II}]\lambda\lambda 6716, 31/\text{H}\alpha$ versus $[\text{O III}]\lambda 5007/\text{H}\beta$, are also included in ITERA as predefined diagnostic diagrams for ease of use.

2.3. Comparison with Observations

Ultimately, the use of ionization models lies in their diagnostic power for observations, which is why ITERA also includes the ability to enter data. To allow for easy comparison of observations with the models, the ITERA program has three simple ways in which data can be entered into the emission-line diagnostic diagrams directly; direct point by point entry, a simple list of line ratios for multiple data, and via tabulated emission line data for multiple line ratio comparisons. For the first two options, the line ratios for the chosen diagram are entered in and compared directly with the model on the chosen line ratio diagram (as shown in figure 2). Once the chosen diagram has cleared or another line ratio diagram chosen, the data are cleared. The tabulated emission line data are chosen in a similar manner as the models, with the data plotted over the model grids if they contain the chosen emission lines. Templates for the tabulated data are available with the ITERA program.

Conversely, the fluxes (relative to $\text{H}\beta$) from the selected model grids for the four emission lines of the chosen line diagnostic diagram can be exported to formatted ASCII files for comparison with observational data. This is especially useful in cases of large datasets, such as with SDSS.

3. Emission Line Ratio Diagnostics

To demonstrate the capabilities of ITERA, we present here three emission-line ratio diagrams covering a range of wavelengths and diagnostic capabilities. These diagrams are all direct output from the ITERA routine, excluding the histogram in the first diagram.

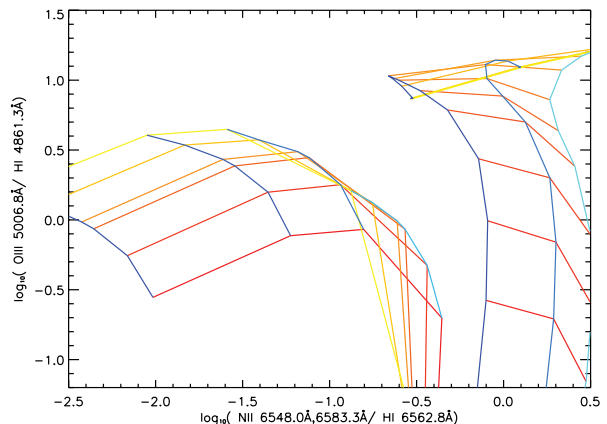


Figure 1: The BPT diagram of $[\text{N II}]/\text{H}\alpha$ versus $[\text{O III}]/\text{H}\beta$, showing grids of photoionization models for star forming galaxies (left, Levesque et al., 2010) and AGN (right, Groves et al., 2004b), described fully in the text. In both grids, lines of constant metallicity are shown by the blue curves, increasing from dark blue to light blue, and lines of constant ionization parameter are shown by the orange curves, increasing in value from red to yellow. In the background is an image of a 2d density diagram from the SDSS DR4 sample described in Groves et al. (2006), showing star-forming galaxies (green), Seyfert galaxies (blue) and LINER galaxies (red).

The first diagram (figure 1) shows $[\text{N II}]/\text{H}\alpha$ versus $[\text{O III}]/\text{H}\beta$, the classic ‘‘BPT’’ diagram from Baldwin et al. (1981) that is a diagnostic of the excitation mechanism in emission-line galaxies. Shown on this plot are two model grids; the Levesque et al. (2010) STD models for star-forming galaxies on the left, and the Groves et al. (2004b) models for Dusty AGN on the right. Both grids show a range of metallicities (blue curves) and ionization parameters (orange curves), though note that these grids are not equivalent. The exact parameters that the star forming models have are: $Z \sim 0.05, 0.2, 0.4, 1.0, 2.0Z_{\odot}$ and $q = 1 \times 10^7, 2 \times 10^7, 4 \times 10^7, 8 \times 10^7, 1 \times 10^8, 2 \times 10^8, 4 \times 10^8 \text{ cm s}^{-1}$, for a 2 Myr old burst with density $n_{\text{H}} = 100 \text{ cm}^{-3}$, while the AGN models have: $Z \sim 1.0, 2.0, 4.0Z_{\odot}$ with $\log \mathcal{U} = 0.0, -0.3, -0.6, -1.0, \dots, -3.6, -4.0$, a gas density of $n_{\text{H}} = 1000 \text{ cm}^{-3}$ and are ionized by a power-law of index $\beta = -1.4$. Underlying the grids is a coloured 2D density histogram of the SDSS DR4 emission line galaxy sample from Groves et al. (2006), displaying the observed distribution of star forming galaxies (Green squares), Seyfert galaxies (blue squares), and LINER galaxies (red squares).

The model grids clearly encompass the observed line ratio space. Note how the star forming mod-

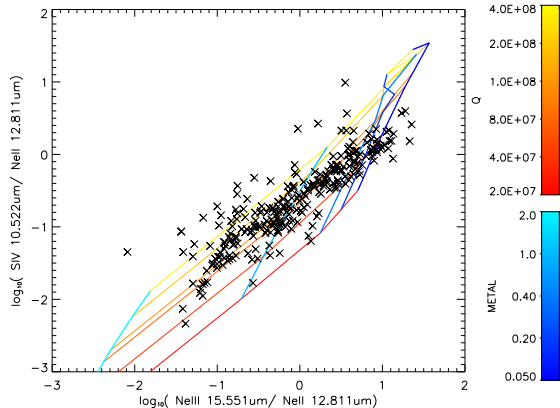


Figure 2: The mid IR emission line ratio diagram of $[\text{Ne III}]15.6\mu\text{m}/[\text{Ne II}]12.8\mu\text{m}$ versus $[\text{S IV}]10.5\mu\text{m}/[\text{Ne II}]12.8\mu\text{m}$, showing the same Levesque et al. (2010) star forming galaxy photoionization model as in figure 1, with the grids curves as labelled in the colour bar to the right. The stars are a sample of O and B star ionized systems (star-forming galaxies and extragalactic and galactic H II systems) collated and described in Groves et al. (2008).

els follow closely the green branch of this diagram, showing the known strong dependence on metallicity of the $[\text{N II}]/\text{H}\alpha$ ratio, with the ionization parameter affecting the position of the models in both ratios, explaining the spread in observed galaxies (along with the average age of the ionizing stars). Also note that the models fail to reproduce the observed line ratios at very low metallicities, and do so even when different ages are used for the ionizing stars, indicating that there are still underlying issues with either the photoionization models, stellar population models, or both. The AGN model grid on the other hand actually tends to be too broad, demonstrating the sparsity of low metallicity AGN in the SDSS emission-line galaxy sample, as discussed in Groves et al. (2006). The low \mathcal{U} NLR models are likely to be too faint to be observed in this sample. It should be remembered that the AGN and star forming galaxy models show are the extremes, of pure AGN contribution and pure H II regions. In between these models, seen in the right-hand wing of the diagram (the ‘AGN’ branch) are galaxies where both mechanisms, active star formation and AGN, contribute to the galaxy spectrum.

The second diagram (figure 2) shows the mid-IR diagram of $[\text{Ne III}]15.6\mu\text{m}/[\text{Ne II}]12.8\mu\text{m}$ versus $[\text{S IV}]10.5\mu\text{m}/[\text{Ne II}]12.8\mu\text{m}$. A surprisingly strong correlation between these ratios was found by

Groves et al. (2008), who explored a large sample of emission line objects to see if the ground-observable $[\text{S IV}]/[\text{Ne II}]$ ratio could replace the space-only, ionization sensitive $[\text{Ne III}]/[\text{Ne II}]$ ratio. Here we show only a sub-sample of that collated by Groves et al. (2008), displaying only star formation ionized regions (starbursts, blue compact dwarfs, extragalactic H II regions, and galactic H II regions), shown as crosses on figure 2. Overlaying the observed data is same star-formation model grid of metallicity and ionization parameter as in figure 1, as labelled in the colour bars. The model grid broadly covers the observations, with both higher metallicity and lower ionization parameter towards the lower left of the grid (lower ionization). This is somewhat degenerate with the age of the ionizing stellar population, with ages greater than ~ 4 Myrs moving strongly to the lower left of the grid.

There are two interesting points to take from this grid. The first is that the models are unable to explain the full spread of the data, though this may arise due to the $\sim 20\%$ uncertainty in the data (see Groves et al., 2008, for details). The high values of $[\text{S IV}]/[\text{Ne II}]$ may come also from higher ionization parameters and or different abundance patterns, but the points to the right of the diagram suggest, as in the previous figure, that the low metallicity models (or youngest age or Wolf-Rayet models similarly) are lacking a hard enough spectrum to reach these ionization states.

The second is that the observed relation between $[\text{Ne III}]/[\text{Ne II}]$ and $[\text{S IV}]/[\text{Ne II}]$ has a different slope and narrower spread than the model grid, suggesting that there may a higher order correlation going on between the metallicity and age of the stellar population and the ionization parameter of the ionized gas.

The final diagram uses optical and far-IR lines of the same species, O^{+2} , aiming towards the ionized gas diagnostics possible with *Herschel Space Telescope*, specifically the PACS spectrometer. Figure 3 shows the $[\text{O III}] 52\mu\text{m}/88\mu\text{m}$ versus $[\text{O III}]5007\text{\AA}/88\mu\text{m}$, based on the Dinerstein et al. (1985) diagram. This diagram is a strong diagnostic diagram, separating out both density and temperature, while avoiding direct abundance and ionization effects. While unfortunately the density sensitive $52\mu\text{m}/88\mu\text{m}$ ratio cannot be observed in the local Universe with *Herschel* due to the lower wavelength limit, the temperature sensitive $5007\text{\AA}/88\mu\text{m}$ ratio can be obtained with the combination of *Herschel* PACS spectra with ground

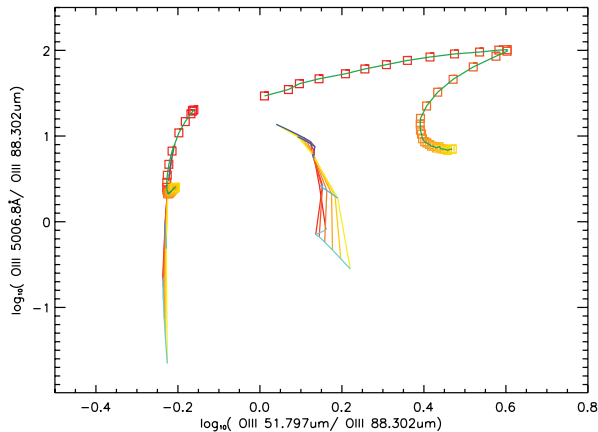


Figure 3: Diagnostic diagram using only O^{+2} emission lines, containing the density sensitive $[O\text{ III}] 52\mu\text{m}/88\mu\text{m}$ ratio versus the temperature sensitive $[O\text{ III}]5007\text{\AA}/88\mu\text{m}$ ratio, that both use the *Herschel* observable $[O\text{ III}]88\mu\text{m}$ line. Shown are two different density ($n_{\text{H}} = 10\text{ cm}^{-3}$, lower left grid, and $n_{\text{H}} = 350\text{ cm}^{-3}$, lower right grid) instantaneous starburst models from Kewley et al. (2001), and two different density ($n_{\text{H}} = 0.1\text{ cm}^{-3}$, upper left green curve, and $n_{\text{H}} = 10\text{ cm}^{-3}$, upper right green curve) shock models from Allen et al. (2008). In both models, the state of ionization (ionization parameter or shock velocity) increases from red to yellow. The four models are well separated in this diagram thanks to the diagnostic power of the ratios.

based data. In reality however, caution must be taken with this ratio, as there are clear difficulties associated with the different wavelengths, such as matching the *Herschel* apertures and pixels with ground based data, and the large difference in dust attenuation between the two lines, both of which effects could overwhelm any small variations due to temperature. Nevertheless, to demonstrate the power of this diagram we show two star forming model grids from Kewley et al. (2001), and two shock model curves from Allen et al. (2008).

The Kewley et al. (2001) models are grids in metallicity (blue curves, same as Levesque models) and ionization parameter (orange curves) using a Starburst99 3 Myr old instantaneous burst as the ionizing source. What distinguishes the two model grids is the density of the ionized gas, with the left grid at $n_{\text{H}} = 10\text{ cm}^{-3}$, and the right grid at $n_{\text{H}} = 350\text{ cm}^{-3}$. The $52\mu\text{m}/88\mu\text{m}$ ratio clearly separates the two grids. Though difficult to see due to their collapsed form, the $5007\text{\AA}/88\mu\text{m}$ ratio is affected by both the ionization parameter (weakly) and the metallicity (more strongly). However the diagnostic strength of this ratio is more clearly seen when compared to the much hotter ionized gas in

the shocks.

The Allen et al. (2008) model curves (green) show pure shock models at solar metallicity, magnetic parameter of $B/\sqrt{n} = 1\mu\text{G cm}^{3/2}$, and velocities ranging from 150 (red squares) – 1000 (yellow squares) km s^{-1} . Note that the velocities are shown as squares due to one of the features of ITERA, where if one of the parameters are set to a single value, in this case solar metallicity, the varying parameter along the curve is marked by squares. As with the Kewley models, the two curves are again separated by density, with the left curve having a pre-shock density of $n_{\text{H}} = 0.1\text{ cm}^{-3}$, and the right $n_{\text{H}} = 10\text{ cm}^{-3}$. What is clearly noticeable in figure 3, is the clear vertical offset between the shock models and star forming models in the temperature sensitive $[O\text{ III}] 5007\text{\AA}/88\mu\text{m}$ ratio, demonstrating clearly the possible capabilities of upcoming *Herschel*-PACS spectral surveys.

4. Summary

We have presented here a new tool to enable astronomers to compare observations of emission line ratios with that determined by photoionization and shock models, ITERA, the IDL Tool for Emission-line Ratio Analysis. ITERA is an IDL widget tool which allows the user to plot ratios of any strong atomic and ionized emission lines as determined by standard photoionization and shock models. These line ratio diagrams can then be used to determine diagnostics for nebulae excitation mechanisms (such as discussed in the Baldwin et al., 1981, paper) or for nebulae parameters such as density, temperature, metallicity, etc. ITERA can also be used to determine line sensitivities to such parameters, compare observations with the models, or even estimate unobserved line fluxes. This tool, and associated libraries and instructions, can be obtained at <http://www.brentgroves.net/itera.html>.

At its core lies a library of emission-line nebulae models, covering photoionization by young O and B stars (e.g. Kewley et al., 2001; Dopita et al., 2006), photoionization by a hard power-law spectrum from an AGN (e.g. Groves et al., 2004b) and ionization by shocks (e.g. Allen et al., 2008). These models broadly cover the space of observed emission-line objects.

Finally, to demonstrate the capabilities of ITERA we present three different line diagnostic diagrams; the classic BPT diagram of $[\text{N II}]\lambda\lambda 6548, 6584/ha$ versus $[\text{O III}]\lambda 5007/\text{H}\beta$,

showing the coverage of the star forming galaxy and AGN photoionization models when compared to SDSS emission-line galaxies, the mid-IR diagram of $[\text{Ne III}]15.6\mu\text{m}/[\text{Ne II}]12.8\mu\text{m}$ versus $[\text{S IV}]10.5\mu\text{m}/[\text{Ne II}]12.8\mu\text{m}$, revealing an interesting correlation of ionization parameter and metallicity of stellar photoionization models when compared to observations, and the optical IR diagram of O^{+2} , $[\text{O III}]52\mu\text{m}/88\mu\text{m}$ versus $[\text{O III}]5007\text{\AA}/88\mu\text{m}$, demonstrating one of the diagnostic possibilities of *Herschel*.

It is hoped that this tool will be of great use to the astronomical community when analyzing spectra of emission-line regions due to both its simplicity and ease of use, especially as the library expands with the growing number of photoionization and shock models becoming available.

Acknowledgements

The authors would like to thank those who have given feedback on ITERA as it was being developed; B. Brandl, E. da Cunha, J. Holt, M. Sarzi and H. Spoon.

Allen, M. G., Groves, B. A., Dopita, M. A., Sutherland, R. S., & Kewley, L. J. 2008, ApJS, 178, 20
 Aller, L. H., Ufford, C. W., & van Vleck, J. H. 1949, ApJ, 109, 42
 Asplund, M., Grevesse, N., & Sauval, A. J. 2005, Cosmic Abundances as Records of Stellar Evolution and Nucleosynthesis, 336, 25
 Baldwin, J. A., Phillips, M. M., & Terlevich, R. 1981, PASP, 93, 5
 Binette, L., Wilson, A. S., & Storchi-Bergmann, T. 1996, A&A, 312, 365
 Brocklehurst, M. 1971, MNRAS, 153, 471
 Cox, D. P., & Mathews, W. G. 1969, ApJ, 155, 859
 Dinerstein, H. L., Lester, D. F., & Werner, M. W. 1985, ApJ, 291, 561
 Dopita, M. A., et al. 2006, ApJS, 167, 177
 Dopita, M. A., & Sutherland, R. S. 2003, Astrophysics of the diffuse universe, Berlin, New York: Springer, 2003. Astronomy and astrophysics library, ISBN 3540433627
 Fioc, M., & Rocca-Volmerange, B. 1997, A&A, 326, 950
 Ferland, G. J., Korista, K. T., Verner, D. A., Ferguson, J. W., Kingdon, J. B., & Verner, E. M. 1998, PASP, 110, 761
 Ferguson, J. W., Korista, K. T., Baldwin, J. A., & Ferland, G. J. 1997, ApJ, 487, 122
 Groves, B. A., Dopita, M. A., & Sutherland, R. S. 2004, ApJS, 153, 9
 Groves, B. A., Dopita, M. A., & Sutherland, R. S. 2004, ApJS, 153, 75
 Groves, B. A., Heckman, T. M., & Kauffmann, G. 2006, MNRAS, 371, 1559
 Groves, B., Nefs, B., & Brandl, B. 2008, MNRAS, 391, L113
 Heckman, T. M. 1980, A&A, 87, 152
 Kauffmann, G., et al. 2003, MNRAS, 346, 1055

Kewley, L. J., Dopita, M. A., Sutherland, R. S., Heisler, C. A., & Trevena, J. 2001, ApJ, 556, 121
 Kewley, L. J., & Dopita, M. A. 2002, ApJS, 142, 35
 Kewley, L. J., Groves, B., Kauffmann, G., & Heckman, T. 2006, MNRAS, 372, 961
 Kewley, L. J., & Ellison, S. L. 2008, ApJ, 681, 1183
 Leitherer, C., et al. 1999, ApJS, 123, 3
 Levesque, E. M., Kewley, L. J., & Larson, K. L. 2010, AJ, 139, 712
 , D. H., Aller, L. H., & Hebb, M. H. 1941, ApJ, 93, 230
 Miller, J. S., & Mathews, W. G. 1972, ApJ, 172, 593
 Morisset, C. 2008, SF2A-2008, 335
 Osterbrock, D. E., & Ferland, G. J. 2006, Astrophysics of gaseous nebulae and active galactic nuclei, 2nd. ed. by D.E. Osterbrock and G.J. Ferland. Sausalito, CA: University Science Books, 2006
 Péquignot, D., et al. 2001, Spectroscopic Challenges of Photoionized Plasmas, 247, 533
 Peimbert, M. 1967, ApJ, 150, 825
 Rubin, R. H. 1989, ApJS, 69, 897
 Seaton, M. J. 1960, Reports on Progress in Physics, 23, 313
 Stasińska, G. 2007, arXiv:0704.0348
 Vázquez, G. A., & Leitherer, C. 2005, ApJ, 621, 695
 Veilleux, S., & Osterbrock, D. E. 1987, ApJS, 63, 295